Identification of a 1-deoxy-D-xylulose-5-phosphate synthase (DXS) mutant with improved crystallographic properties

Robin M. Gierse [a, b, c, 1], Eswar R. Reddem [c, d, 1], Alaa Alhayek [a, b], Dominik Baitinger [a], Zhoor Hamid [a, b], Harald Jakobi [e], Bernd Laber [e], Gudrun Lange [e], Anna K.H. Hirsch [a, b, c, **], Matthew R. Groves [d, *]

[a] Department for Drug Design and Optimization, Helmholtz Institute for Pharmaceutical Research (HIPS) — Helmholtz Centre for Infection Research (HZI), Campus Building E 8.1, 66123, Saarbrücken, Germany
[b] Department of Pharmacy, Saarland University, Campus Building E8.1, 66123, Saarbrücken, Germany
[c] Stratingh Institute for Chemistry, University of Groningen, Nijenborgh 7, 9747, AG Groningen, Netherlands
[d] Pharmacy Department, Drug Design Group, University of Groningen, Antonius Deusinglaan 1, 9700, AV Groningen, Netherlands
[e] Research & Development Crop Science, Bayer AG, Industriepark Höchst, 65926, Frankfurt, Germany

ARTICLE INFO

ABSTRACT

In this report, we describe a truncated Deinococcus radiodurans 1-deoxy-D-xylulose-5-phosphate synthase (DXS) protein that retains enzymatic activity, while slowing protein degradation and showing improved crystallization properties. With modern drug-design approaches relying heavily on the elucidation of atomic interactions of potential new drugs with their targets, the need for co-crystal structures with the compounds of interest is high. DXS itself is a promising drug target, as it catalyzes the first reaction in the 2-C-methyl-D-erythritol 4-phosphate (MEP)-pathway for the biosynthesis of the universal precursors of terpenes, which are essential secondary metabolites. In contrast to many bacteria and pathogens, which employ the MEP pathway, mammals use the distinct mevalonate-pathway for the biosynthesis of these precursors, which makes all enzymes of the MEP-pathway potential new targets for the development of anti-infectives. However, crystallization of DXS has proven to be challenging: while the first X-ray structures from Escherichia coli and D. radiodurans were solved in 2004, since then only two additions have been made in 2019 that were obtained under anoxic conditions. The presented site of truncation can potentially also be transferred to other homologues, opening up the possibility for the determination of crystal structures from pathogenic species, which until now could not be crystallized. This manuscript also provides a further example that truncation of a variable region of a protein can lead to improved structural data.

1. Introduction

In 2015, the world health organization (WHO) published a

global action plan on antimicrobial resistance (AMR) [1]. One of the five main objectives in the plan is an increase of research and development to fight AMR. In addition to improvements in how available antibiotics can be used, the development of innovative drugs is an essential strategy to address emerging resistance. The 2019 WHO report on antibacterial agents in clinical development defines the required innovation of a drug by the absence of cross-resistance, a new compound or target class or a new mode of inhibition. The authors estimate that in the next five years, eleven new antibiotics could be approved, but only one might be innovative and active against resistant Gram-negative bacteria - highlighting that the need for innovative antibiotics is as urgent as ever [2].

The targets of antibiotics currently on the market have been

mainly involved in mechanisms essential for the proliferation of pathogens, such as protein and cell-wall biosynthesis or DNA/RNA replication and repair [3]. Nowadays, in the search for innovative antibiotics, more and more unconventional targets are explored. One source for unconventional targets is the methylerythritol-phosphate (MEP)-pathway. Before the discovery of this pathway in 1993, its products, isopentenyl diphosphate and dimethylallyl diphosphate, were thought to be exclusively accessible via the mevalonate pathway [4—6]. With the discovery of the MEP pathway, an alternative biosynthetic route to these universal building blocks for all isoprenoids was found. Many bacteria and the chloroplasts of plants rely on this pathway, whereas humans and most Eukarya use the mevalonate pathway [5—7]. This distinction amongst species makes the MEP pathway very attractive for the development of new drugs [8,9]. As a result, the MEP pathway has been the target of several projects to develop new antibiotics [10—12].

The first enzyme of the MEP pathway, 1-deoxy-D-xylulose-5-phosphate synthase (DXS), catalyzes the rate-limiting formation of 1-deoxy-d-xylulose 5-phosphate (DOXP) [13]. Compared with all other downstream intermediates, DOXP offers the additional benefit of being also the starting material for the biosynthesis of thiamine diphosphate (vitamin B1) and pyridoxal 5-phosphate (vitamin B6) [14,15]. As DXS is also involved in multiple essential biosynthetic routes, we selected the enzyme DXS as a strategic branch point and therefore as a particularly interesting target for our own drug development [16,17].

Modern hit-identification strategies benefit greatly from structural knowledge of the enzymatic target, and drug optimization is accelerated by detailed knowledge of the atomic interactions between the compounds of interest with its target. However, while DXS has long been a target of interest, there is a relative paucity of high resolution structural information on this target: the first two crystal structures from organisms *Escherichia coli* and *Deinococcus radiodurans* were published in 2007, at highest resolution of 2.4 Å [18]. Notably, Xiang et al. reported that the DXS protein of *E. coli* was only crystallized successfully after a fungal contamination led to partial proteolysis of the enzyme [18,19]. Due to the potential of the MEP pathway for the development of new antibiotics, the demand for additional structural information of DXS homologues is high. This is illustrated by reports on the computation of homology models of pathogenic organisms, such as *Mycobacterium tuberculosis* and *Plasmodium falciparum* [20,21], and the use of orthogonal methods to gain structural insights, such as H/D exchange MS [22]. In 2019, two DXS crystal structures of *D. radiodurans* were solved to higher resolution (1.95 Å) by Drennan and coworkers [23]. These structures give further insight on the catalytic steps of DXS, but crystals must be grown under anoxic conditions, limiting the functional states of the enzyme that can be structurally characterized.

To support our own structure-based drug-design projects, we developed a truncated DXS construct that crystallizes readily under aerobic conditions and diffracts to a resolution of 2.10 Å. The truncated loop has a very low evolutionary conservation and we show that its removal had no influence on enzymatic activity. Due to the low conservation of the identified region, a similar approach should also be applicable to homologues of DXS, enabling the determination of crystal structures from pathogenic organisms in the future.

2. Materials and methods

2.1. Protein expression and purification

The truncated DXS gene was obtained commercially, cloned into the pETM-11 expression vector and transformed into *Escherichia coli* BL21 (DE3). drDXS and ΔdrDXS were expressed and purified as described by Xiang et al. with minor modifications [18]. After IMAC and Ion-exchange chromatography, the ΔdrDXS-containing fractions were pooled and cleavage of the His-tag was performed by TEV-protease digestion at 4 °C overnight. Removal of the tag and protease was achieved by reversed IMAC chromatography. After concentration by ultrafiltration using a VivaSpin ultrafiltration device with a molecular weight cut-off of 30 kDa, the final gel filtration chromatography of ΔdrDXS was performed in 20 mM Tris-HCl (pH 7.5) 150 mM NaCl, 10 mM DTT.

2.2. Crystallization

The protein was concentrated in the presence of 50 μM ThDP to 23 mg/mL by ultrafiltration. The sample was centrifuged at 14,000 rpm before setting up drops. Initial screening was performed using commercial screens at RT in 96-well, SDMRC2 sitting-drop plates. For optimization, crystals were grown at RT using 2 μL hanging-drops, 1:1 mixture of protein and mother liquor. Crystals were obtained after 48 h with 0.2 M calcium acetate hydrate, 0.1 M Tris pH 8.5 and 20% PEG 4000 as the precipitant.

2.3. Data collection, processing and refinement

Diffraction data were collected at beamlines P11 and P13, DESY, Hamburg. Data reduction and scaling was performed using XDS [24]. Molecular replacement with Molrep was used for phasing, using 2o1x as a search model [25]. The model was further refined during several rounds of iterative manual model building and refinement in the CCP4 suite using coot and refmac [26—28]. Refinement statistics are shown in Table S1.

2.4. Kinetic measurements

The DXS activity was analyzed at RT as previously reported, with minor modifications [29,30]. Assay volume was 60 μL, to enable the use of 384-well plates (Greiner BioOne), buffer was 200 mM HEPES, pH 8.0. Data analysis was performed with the enzyme kinetics module of Origin pro 2019.

2.5. Thermal-shift assay (TSA)

Analysis was performed using an ABI StepOneplus RT-PCR instrument using white 96-well plates. A continuous heating rate of 1 °C/min from 20 °C to 95 °C was used. Sample volume was 25 μL, consisting of 20 μL TSA buffer (20 mM Tris-HCl, pH 8.0; 300 mM NaCl, 5 mM MgCl$_2$), 2.5 μL protein solution and 2.5 μL dye (Sypro Orange, 5000 x in DMSO, Sigma-Aldrich). Optimal concentrations were experimentally determined, 1 mg/mL of protein, 50 x Sypro Orange in TSA buffer yielded the best signal-to-noise ratio.

2.6. LC-MS measurements

The protocol for LC-MS measurements is provided, together with its results, in the SI.

3. Results and discussion

3.1. Truncation strategy used to design a crystallizing protein construct of DXS

While reproducing the protein crystals of *D. radiodurans* DXS (drDXS), we have observed a partial proteolysis of the 67 kDa protein into fragments of 20 and 40 kDa size, as previously reported

for *E. coli* and *P. aeruginosa* DXS (Fig. S1) [18,31]. This prompted us to use the technique of limited proteolysis to optimize the DXS protein. This method is based on the observation that well-structured domains of a protein are protected against proteolytic digestion [32,33]. Analysis of such a partial digestion can lead to re-engineered proteins that contain the protected, well-folded domains and have often more suitable properties for protein crystallography.

In the case of DXS, while a digestion site is not identified in the published crystal structures, amino acids 199—244 show no electron density in the DXS structures 6ouw, 2o1x and 2o1s and only fragmented, partial density for 6ouv. As a result, we hypothesized that the 20 kDa fragment corresponds to amino acids 1—199 and the 40 kDa fragment to amino acids 240—629. The degraded protein sample was analyzed by LC-MS to identify the exact cleavage site. A ~20 kDa fragment could not be observed, but we could observe a mixture of three different species with masses of 42,890, 42,690 and 42,489 Da, respectively (Fig. S2, S3). The observed masses correspond well to the calculated masses of the drDXS protein fragments with the amino acids 232, 234 or 236 to 629, respectively (sequence following UniProt-ID: Q9RUB5). Taken together, we concluded that the loop of amino acids 199—236 of drDXS is particularly sensitive to proteases, but we cannot exclude the possibility of autocatalytic cleavage of this loop.

To answer the question if the flexible loop is a species-independent property of the DXS enzyme, we analyzed the sequence conservation of all 498 deposited and manually annotated bacterial DXS genes of the Uniprot database [34]. A simplified image of the calculated multiple sequence alignment (MSA) is shown in Fig. 1 (full MSA in **SI**). While the sequence homology of all 498 DXS proteins is 62.6% overall, the digested loop (200—232) displays a lower homology of 41.2%. We found that the loop also has a high variability in length, ranging from 5 to 58 amino acids in Myxococcus xanthus and Kocuria rhizophila, respectively. The mean loop length is with 45 amino acids similar to that of the 43 amino acids of *D. radiodurans*. Such variability is an indication that this loop is not essential for the catalytic reaction.

Based on the LC-MS results, the MSA and the lack of density between amino acids 200—240 in 2o1x, we designed a construct that replaces amino acids 201—243 with six glycine residues. This linker was designed to be long enough to bridge the gap of 11.7 Å between the two amino acid chains, but short enough to avoid introduction of multiple linker conformations. We expected that these modifications yield an optimized protein (ΔdrDXS), with properties more suitable for crystallization (sequence in SI).

3.2. Biophysical characterization

Purified ΔdrDXS protein was analyzed by LC-MS. The sample eluted as a single peak with a mass of 63,382.95 Da, which is in good agreement with the calculated mass for ΔdrDXS of 63,382.11 Da (Fig. S4). LC-MS and SDS-PAGE analysis showed the intact protein, even after a week incubation at RT, confirming the desired improvement in stability of ΔdrDXS (Fig. S1, S4).

To analyze if the truncation affects the activity of ΔdrDXS, we determined the enzyme kinetics for both substrates [31]. The results are summarized in Table 1 and shown in Fig. S6, S7. The truncated drDXS enzyme retains its catalytic activity. It shows, however, slightly lower affinities for both substrates and a reduced turnover number.

To further investigate the effects of the truncation, the melting points (T_m) were determined using a thermal shift assay (TSA) [35], in which any increase of the T_m is a sign of improved protein stability. This is often used to screen for optimal buffer conditions or analyze the effect of mutations [36]. With a T_m of 55.2 °C, the truncated enzyme shows a nearly identical value to that of the native enzyme, which has a T_m of 55.0 °C (Fig. S8), indicating that our loop truncation had no significant effect on protein stability.

Crystallization screening of ΔdrDXS yielded several conditions, with the best crystals diffracting to a resolution of 2.1 Å. The protein structure obtained is deposited in the PDB with the code 6xxg and the collection and refinement statistics are reported in Table S1.

3.3. Effects of the truncation on protein folding

The truncated protein is catalytically active and no major changes in its properties could be identified using biophysical characterization methods. Since the ΔdrDXS protein yields well-diffracting protein crystals, we were also able to analyze the effect of the truncation by comparison of the obtained X-ray structure with the wild-type enzyme.

To compare the structures, the C_α-RMSD of residues 8—183, 253—288 and 322—627 between truncated and the wild-type structures were calculated, and a superposition colored by individual C_α-RMSD is shown in Fig. 2 [26,37]. The RMSD on C-alpha position is 0.459 Å, 0.476 Å and 0.328 Å with 2o1x, 6ouv and 6ouw, respectively. These values show that the majority of the structure is unaffected by the truncation. While comparing the structures, we could also identify two regions that are present in a novel conformation: an α-helix (residues 186—200) and a β-hairpin motif (residues 303—320; Fig. 2).

The β-hairpin motif (residues 303—320) was described recently as part of a so-called "spoon". This motif undergoes structural
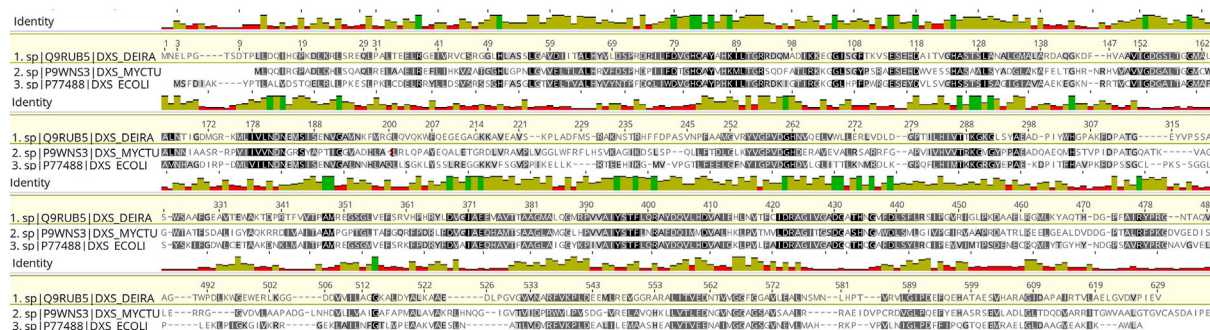

Fig. 1. MSA of DXS enzymes, including *Deinococcus radiodurans* (1, DEIRA) and *Mycobacterium tuberculosis* (2, MYCTU). For the sake of clarity, the image only shows three sequences. The identity, shown as bar graph above the sequences, was calculated using all 498 aligned sequences. Between amino acids 200 and 240, a highly variable region can be observed.

Table 1
Kinetic comparison of the native and truncated drDXS enzyme.

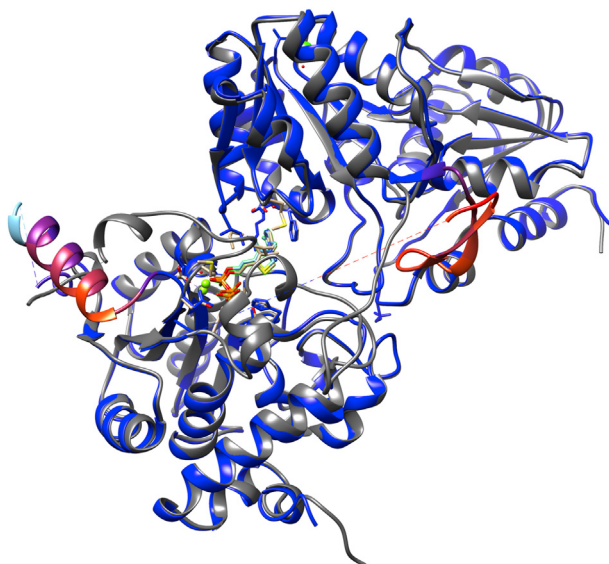|	Pyruvate	D-GAP
drDXS	K_m: 58 ± 9 μM v_{max}: 2.2 μmol/min k_{cat}: 0.78 s^{-1}	K_m: 193 ± 23 μM v_{max}: 1.8 μmol/min k_{cat}: 0.64 s^{-1}
ΔdrDXS	K_m: 85 ± 9 μM v_{max}: 2.6 μmol/min k_{cat}: 0.46 s^{-1}	K_m: 260 ± 16 μM v_{max}: 2.3 μmol/min k_{cat}: 0.38 s^{-1}

Fig. 2. Superimposition of the drDXS structures with the code 2o1x (gray) and 6xxg (colored by C$_\alpha$-RMSD). Color coding: blue — low RMSD to red — high RMSD. (For interpretation of the references to color in this figure legend, the reader is referred to the Web version of this article.)

rearrangements during the catalytic cycle of the DXS enzyme upon pyruvate binding. In our structure, the β-sheets of chain A adopt a conformation similar to the reported "bent spoon"-motif, while the equivalent residues of chain B are disordered. However, the "bent spoon" of our structure is distinct from than reported by Drennan and coworkers in 6ouw [23]. With this observation, the presented structure further contributes to the understanding of conformational changes in this region during catalysis.

The α-helix formed by residues 186—200 is directly adjacent to the truncated amino acids 201—243. It can also be observed in the wild-type structure, but starting at residue 193. The C-terminal extension of the helix alters its orientation and moves residues 184—188 away from the ThDP binding site. The amino acids folding away from the active site do not take part in the catalyzed reaction, but form the hydrophobic surface of the ThDP binding site.

The same conformational change of this α-helix can also be observed in the recently published structure 6ouw. In this structure, the amino acids from position 184 are also part of the α-helix and point away from the active site. This similar folding to the truncated structure shows that this conformational change is not caused by the truncation. Jordan and coworkers have also identified the amino acids 183—199 as flexible and solvent-exposed using H/D exchange MS experiments. They show that this part of the protein adopts two distinct states, driven by substrate binding [22]. It seems that the truncation facilitates the formation of a stable α-helix.

3.4. Crystal contacts and packing

We could observe that the residues 186—200 of the α-helix form new lattice contacts. The α-helix of chain A is at a distance of 8 Å and parallel to an α-helix formed by the amino acids 28—46 of an adjacent DXS protein. This proximity enables salt bridges between Asn195 and Arg199 and the Glu35 of the neighboring protein in the crystal lattice with a distance of 2.7 Å and 4.5 Å, respectively (Fig. S9). In future constructs, these interactions could be strengthened by introduction of more charged amino acids.

Comparing the packing, we could identify two different forms of DXS protein crystals. The previously determined structures 2o1x and 6ouv both have a Matthew's coefficient (V$_M$) of 2.75 Å^3/Da and a solvent content of 55%. The truncated structure has a V$_M$ of 2.27 Å^3/Da and a solvent content of 45%, similar to the DXS structure of 6ouw. As shown in Fig. 3, these two proteins adopt a different orientation in the crystal lattice and have a tighter packing, reducing the unit cell parameters. In the tightly packed structure 6ouw, the residues 307—319 are in the "bent-spoon" conformation, in the truncated structure a similar ß-hairpin, but at a location 14 Å distant to the "bent spoon" motif, can be seen. Both structures have the previously described α-helixes of the "fork" motif (amino acids 292—306) in a disordered state with no observable electron density.

A higher density in protein crystals correlates with an increased resolution and is a desirable feature for future crystal structures in complex with ligands [38,39]. Using the truncated protein and the addition of pyruvate during crystallization seems to push the protein into the "bent spoon" conformation and might be used in the future to obtain better protein crystals. With a sample size of only four protein crystals, this hypothesis will need further evaluation as more DXS structures become available.

4. Conclusion

In our efforts to create a DXS enzyme for crystallographic studies with improved stability, we identified the part of the enzyme that is most susceptible to degradation. The identified loop is comprised of the residues 201—243, which show a high evolutionary variability in both length and sequence through all known bacterial homologues. We designed and expressed a mutant protein lacking the identified loop. The truncation showed only a small effect on the enzymatic activity and no effect on the biophysical properties of DXS, but a substantial improvement in the crystallographic properties of the protein. The ΔdrDXS protein has an improved tendency to form protein crystals under aerobic conditions, and diffract to a better resolution than previously published aerobic crystals of the wild-type protein.

Comparison of the obtained crystal structure with published structures showed no effect of the truncation on the remaining protein. Only two regions of the enzyme, previously known to be flexible, were identified in a different conformation and give additional evidence for the recently reported "spoon"/"fork" motif at the active site, proposed by Drennan and coworkers [23].

As we could find this loop in all species, we expect that the transfer of the identified site of truncation to other bacterial
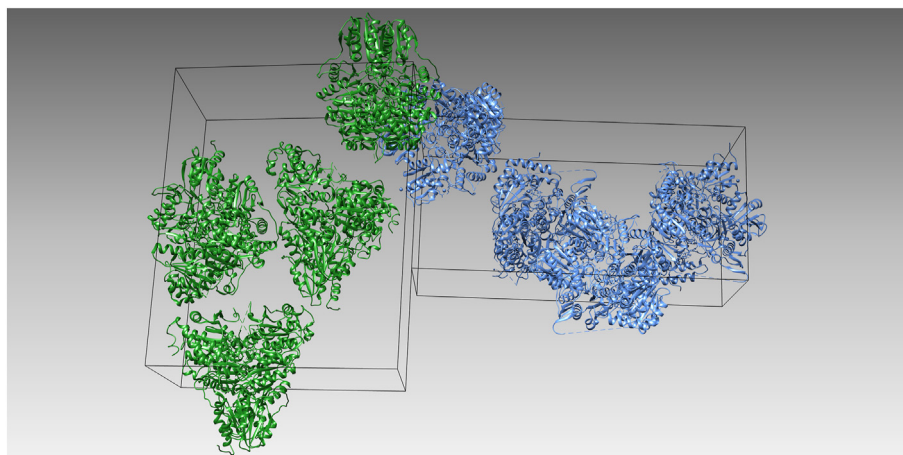
Fig. 3. Left, green: Unit cell of the drDXS enzyme in the 2o1x and 6ouv crystal structures. Cell size is $78 \times 125 \times 151$ Å with a volume of 1.47×10^6 Å^3; right, blue: Unit cell of ΔdrDXS. Unit cell parameters are with $72 \times 87 \times 181$ Å resulting in a smaller volume of 1.13×10^6 Å^3. (For interpretation of the references to color in this figure legend, the reader is referred to the Web version of this article.)

homologues will show comparable effects. The MSA that we supply in the SI can be used by other research groups interested in DXS to design similar truncated homologues proteins with improved properties. We expect that this will facilitate the determination of DXS crystal structures from relevant pathogens.

Declaration of competing interest

The authors declare that they have no known competing financial interests or personal relationships that could have appeared to influence the work reported in this paper.

Acknowledgments

Appendix A. Supplementary data

Supplementary data to this article can be found online at https://doi.org/10.1016/j.bbrc.2020.12.069.

Funding

References

[1] Global Action Plan on Antimicrobial Resistance, Microbe Mag 10 (2015) 354—355, https://doi.org/10.1128/microbe.10.354.1.

[2] W.H.O.WHO, World Health Organization, Antibacterial Agents in Clinical Development: an Analysis of the Antibacterial Clinical Development Pipeline, 2019, 2019.

[3] C. Walsh, A.S. for Microbiology, Antibiotics: Actions, Origins, Resistance, ASM Press, 2003.

[4] M. Rohmer, M. Seemann, S. Horbach, et al., Glyceraldehyde 3-phosphate and pyruvate as precursors of isoprenic units in an alternative non-mevalonate pathway for terpenoid biosynthesis, J. Am. Chem. Soc. 118 (1996) 2564—2566, https://doi.org/10.1021/ja9538344.

[5] H.K. Lichtenthaler, M. Rohmer, J.S. Lichtenthaler, et al., Two independent biochemical pathways for isopentenyl diphosphate and isoprenoid biosynthesis in higher plants, Physiol. Plantarum 101 (1997) 643—652.

[6] M. Rohmer, M. Knani, P. Simonin, et al., Isoprenoid biosynthesis in bacteria: a novel pathway for the early steps leading to isopentenyl diphosphate, Biochem. J. 295 (1993) 517—524, https://doi.org/10.1042/bj2950517.

[7] W.N. Hunter, The non-mevalonate pathway of isoprenoid precursor biosynthesis, J. Biol. Chem. 282 (2007) 21573—21577, https://doi.org/10.1074/jbc.R700005200.

[8] T. Masini, A.K.H. Hirsch, Development of inhibitors of the 2C-methyl-D-erythritol 4-phosphate (MEP) pathway enzymes as potential anti-infective agents, J. Med. Chem. 57 (2014) 9740—9763, https://doi.org/10.1021/jm5010978.

[9] S. Heuston, M. Begley, C.G.M. Gahan, et al., Isoprenoid biosynthesis in bacterial pathogens, Microbiol. (United Kingdom) 158 (2012) 1389—1401, https://doi.org/10.1099/mic.0.051599-0.

[10] C. Mueller, J. Schwender, J. Zeidler, et al., Properties and inhibition of the first two enzymes of the non-mevalonate pathway of isoprenoid biosynthesis, Biochem. Soc. Trans. 28 (2000) 792—793, https://doi.org/10.1042/bst0280792.

[11] J.M. Smith, N. V Warrington, R.J. Vierling, et al., Targeting DXP synthase in human pathogens: enzyme inhibition and antimicrobial activity of butylacetylphosphonate, J. Antibiot. (Tokyo) 67 (2014) 77—83, https://doi.org/10.1038/ja.2013.105.

[12] D. Bartee, S. Sanders, P.D. Phillips, et al., Enamide prodrugs of acetyl phosphonate deoxy- d -xylulose-5-phosphate synthase inhibitors as potent antibacterial agents, ACS Infect. Dis. 5 (2019) 406—417, https://doi.org/10.1021/acsinfecdis.8b00307.

[13] J.M. Estévez, A. Cantero, A. Reindl, et al., 1-Deoxy-D-xylulose-5-phosphate synthase, a limiting enzyme for plastidic isoprenoid biosynthesis in plants, J. Biol. Chem. 276 (2001) 22901—22909, https://doi.org/10.1074/jbc.M100854200.

[14] Q. Du, H. Wang, J. Xie, Thiamin (vitamin B1) biosynthesis and regulation: a rich source of antimicrobial drug targets? Int. J. Biol. Sci. 7 (2011) 41—52, https://doi.org/10.7150/ijbs.7.41.

[15] I.B. Müller, J.E. Hyde, C. Wrenger, Vitamin B metabolism in Plasmodium falciparum as a source of drug targets, Trends Parasitol. 26 (2010) 35—43, https://doi.org/10.1016/j.pt.2009.10.006.

[16] DXS as a target for structure-based drug design, Future Med. Chem. 9 (2017) 1277—1294, https://doi.org/10.4155/fmc-2016-0239.

[17] T. Masini, B.S. Kroezen, A.K.H. Hirsch, Druggability of the enzymes of the non-mevalonate-pathway, Drug Discov. Today 18 (2013) 1256—1262, https://doi.org/10.1016/j.drudis.2013.07.003.

[18] S. Xiang, G. Usunow, G. Lange, et al., Crystal structure of 1-Deoxy-D-xylulose 5-phosphate synthase, a crucial enzyme for isoprenoids biosynthesis, J. Biol. Chem. 282 (2007) 2676—2682, https://doi.org/10.1074/jbc.M610235200.

[19] C.R. Mandel, D. Gebauer, H. Zhang, et al., A serendipitous discovery that in situ proteolysis is essential for the crystallization of yeast CPSF-100 crystallization communications, Acta Crystallogr. F 62 (2006) 1041—1045, https://doi.org/10.1107/S1744309106038152.

[20] A.M. Goswami, Computational analysis, structural modeling and ligand binding site prediction of Plasmodium falciparum 1-deoxy-D-xylulose-5-phosphate synthase, Comput. Biol. Chem. 66 (2017) 1—10, https://doi.org/10.1016/j.compbiolchem.2016.10.010.

[21] T. Masini, B. Lacy, L. Monjas, et al., Validation of a homology model of Mycobacterium tuberculosis DXS: rationalization of observed activities of thiamine derivatives as potent inhibitors of two orthologues of DXS, Org. Biomol. Chem. 13 (2015) 11263—11277, https://doi.org/10.1039/c5ob01666e.

[22] J. Zhou, L. Yang, A. DeColli, et al., Conformational dynamics of 1-deoxy-d-xylulose 5-phosphate synthase on ligand binding revealed by H/D exchange MS, Proc. Natl. Acad. Sci. Unit. States Am. 114 (2017) 9355–9360, https://doi.org/10.1073/pnas.1619981114.

[23] P.Y.T. Chen, A.A. DeColli, C.L. Freel Meyers, et al., X-ray crystallography–based structural elucidation of enzyme-bound intermediates along the 1-deoxy-D-xylulose 5-phosphate synthase reaction coordinate, J. Biol. Chem. 294 (2019) 12405–12414, https://doi.org/10.1074/jbc.RA119.009321.

[24] W. Kabsch, XDS, Acta Crystallogr. D D66 (2010) 125–132, https://doi.org/10.1107/S0907444909047337.

[25] A. Vagin, A. Teplyakov, MOLREP : an automated program for molecular replacement, J. Appl. Crystallogr. 30 (1997) 1022–1025, https://doi.org/10.1107/S0021889897006766.

[26] P. Emsley, B. Lohkamp, W.G. Scott, et al., Features and development of coot, Acta Crystallogr. Sect. D Biol. Crystallogr. 66 (2010) 486–501, https://doi.org/10.1107/S0907444910007493.

[27] M.D. Winn, C. Charles, K.D. Cowtan, et al., Overview of the CCP 4 Suite and Current Developments, vol. 4449, 2011, pp. 235–242, https://doi.org/10.1107/S0907444910045749.

[28] G.N. Murshudov, A.A. Vagin, E.J. Dodson, Refinement of macromolecular structures by the maximum-likelihood method, Acta Crystallogr. D D53 (1997) 240–255, https://doi.org/10.1107/S0907444996012255.

[29] T. Masini, J. Pilger, B.S. Kroezen, et al., De novo fragment-based design of inhibitors of DXS guided by spin-diffusion-based NMR spectroscopy, Chem. Sci. 5 (2014) 3543–3551, https://doi.org/10.1039/c4sc00588k.

[30] S. Hecht, J. Wungsintaweekul, F. Rohdich, et al., Biosynthesis of Terpenoids : efficient multistep biotransformation procedures affording isotope-labeled 2 C -methyl- D -erythritol 4-phosphate using recombinant 2 C -methyl- D -erythritol 4-phosphate, Synthase 61 (2001) 7770–7775, https://doi.org/10.1021/jo015890v.

[31] B. Altincicek, M. Hintz, S. Sanderbrand, et al., Tools for discovery of inhibitors of the 1-deoxy-D-xylulose 5-phosphate (DXP) synthase and DXP reductoisomerase: an approach with enzymes from the pathogenic bacterium Pseudomonas aeruginosa, FEMS Microbiol. Lett. 190 (2000) 329–333, https://doi.org/10.1016/S0378-1097(00)00357-8.

[32] S.L. Cohen, B.T. Chait, A.R. Ferré-D'Amaré, et al., Probing the solution structure of the DNA-binding protein Max by a combination of proteolysis and mass spectrometry, Protein Sci. 4 (1995) 1088–1099, https://doi.org/10.1002/pro.5560040607.

[33] A. Dong, Structure of human DNMT2, an enigmatic DNA methyltransferase homolog that displays denaturant-resistant binding to DNA, Nucleic Acids Res. 29 (2001) 439–448, https://doi.org/10.1093/nar/29.2.439.

[34] A. Bateman, UniProt: a worldwide hub of protein knowledge, Nucleic Acids Res. 47 (2019) D506–D515, https://doi.org/10.1093/nar/gky1049.

[35] U.B. Ericsson, B.M. Hallberg, G.T. DeTitta, et al., Thermofluor-based high-throughput stability optimization of proteins for structural studies, Anal. Biochem. 357 (2006) 289–298, https://doi.org/10.1016/j.ab.2006.07.027.

[36] S. Boivin, S. Kozak, R. Meijers, Optimization of protein purification and characterization using Thermofluor screens, Protein Expr. Purif. 91 (2013) 192–206, https://doi.org/10.1016/j.pep.2013.08.002.

[37] E.F. Pettersen, T.D. Goddard, C.C. Huang, et al., UCSF chimera — a visualization system for exploratory research and analysis, J. Comput. Chem. 25 (2004) 16ß5–1612, https://doi.org/10.1002/jcc.20084.

[38] K.A. Kantardjieff, Matthews Coefficient Probabilities: Improved Estimates for Unit Cell Contents of Proteins, DNA, and Protein − Nucleic Acid Complex Crystals, 2003, pp. 1865–1871, https://doi.org/10.1110/ps.0350503.tially.

[39] B.W. Matthews, Solvent content of protein crystals, J. Mol. Biol. 33 (1968) 491–497, https://doi.org/10.1016/0022-2836(68)90205-2.